tration for $Ta = 10^{10}$ when $\delta \geq O(10)$. In the case of the jovian atmosphere, if we take $Ta = 10^{12}$ for Jupiter (*9*), we obtain $\delta = 100$.

Teleconvection may have important implications for the dynamics of planetary and stellar atmospheres and interiors. According to the structural models of Jupiter by Guillot *et al*. (*1*), regions in the outer part of Jupiter's atmosphere may be stable against convection. Although Earth's liquid core is convectively unstable to convection [e.g., (*5, 6, 17, 21*)] and generates a magnetic field, the outermost part of Earth's core may be stably stratified [e.g., (*22*)]. Our findings suggest that the flows observed on Jupiter (*23, 24*) or the core flows near Earth's core-mantle boundary inferred from geomagnetic observations may be driven by thermal forcing in inner unstable regions rather than by thermal forcing at the sites of the motions themselves. Generally speaking, whenever a convective system is characterized by rapid rotation, low viscosity, and spherical geometry, teleconvection can occur. Convective fluid motions observed on an outer spherical surface may be driven by a deep energy source.

References and Notes

1. T. Guillot, D. Gautier, G. Chabrier, B. Mooser, *Icarus* **112**, 337 (1994).
2. G. Veronis, *Astrophys. J.* **137**, 641 (1963).
3. R. D. Baker, G. Schubert, P. W. Jones, *J. Atmos. Sci.* **55**, 3 (1998).
4. B. Straughan, *Mathematical Aspects of Penetrative Convection* (Longman Scientific, New York, 1993).
5. P. H. Roberts, *Philos. Trans. R. Soc. London Ser. A* **263**, 93 (1968).
6. F. H. Busse, *J. Fluid Mech.* **44**, 441 (1970).
7. K. Zhang, F. Busse, *Geophys. Astrophys. Fluid Dyn.* **39**, 119 (1987).
8. Z. P. Sun, G. Schubert, G. A. Glatzmaier, *Geophys. Astrophys. Fluid Dyn.* **69**, 95 (1993).
9. J. B. Manneville, P. L. Olson, *Icarus* **122**, 242 (1996).
10. C. A. Jones, A. M. Soward, A. I. Mussa, *J. Fluid Mech.* **405**, 157 (2000).
11. K. Zhang, G. Schubert, *Science* **273**, 941 (1996).
12. S. Chandrasekhar, *Hydrodynamic and Hydromagnetic Stability* (Clarendon, Oxford, 1961).
13. A. Tilgner, F. H. Busse, *J. Fluid Mech.* **332**, 359 (1997).
14. K. Zhang, *J. Fluid Mech.* **236**, 535 (1992).
15. P, T, and Θ are governed by three nondimensional equations,

$$[(\nabla^2 - \partial/\partial t)L^2 + Ta^{1/2}\partial/\partial\phi]\nabla^2 P + Ta^{1/2}DT - RL^2\Theta = -\mathbf{r}\cdot\nabla\times\nabla\times(\mathbf{u}\cdot\nabla\mathbf{u})$$

$$[(\nabla^2 - \partial/\partial t)L^2 + Ta^{1/2}\partial/\partial\phi]T - Ta^{1/2}DP = \mathbf{r}\cdot\nabla\times(\mathbf{u}\cdot\nabla\mathbf{u})$$

$$(\nabla^2 - Pr\partial/\partial t)\Theta + L^2(P/r)\partial\Theta_0/\partial r = Pr\mathbf{u}\cdot\nabla\Theta$$

where the differential operator D is defined as

$$D = \mathbf{k}\cdot\nabla - {}^1\!/_2(L^2\mathbf{k}\cdot\nabla + \mathbf{k}\cdot\nabla L^2)$$

with $\mathbf{k}$ a unit vector along the polar axis in the direction of rotation. Nonlinear terms on the right side of the above equations are neglected in our calculations. We impose impenetrable, perfectly thermally conducting, and stress-free boundary conditions

$$P = \Theta = \partial^2 P/\partial r^2 = \partial/\partial r(T/r) = 0$$

at the spherical surfaces $r = r_i$ and $r = r_o$. After applying the standard procedure of the spectral method, convection solutions described by T, P, Θ, the critical Rayleigh number, and the drift rate are obtained by a nonlinear iterative method (*16*).
16. K. Zhang, *J. Fluid Mech.* **268**, 211 (1994).
17. H. K. Moffatt, *Magnetic Field Generation in Electrically Conducting Fluids* (Cambridge Univ. Press, Cambridge, 1978).
18. F. H. Busse, *Icarus* **20**, 255 (1976).
19. ———, *Geophys. Astrophys. Fluid Dyn.* **23**, 152 (1983).
20. M. Ardes, F. H. Busse, J. Wicht, *Phys. Earth Planet. Inter.* **99**, 55 (1997).
21. P. Olson, J. Aurnou, *Nature* **402**, 170 (1999).
22. D. Gubbins, C. J. Thomson, K. A. Whaler, *Geophys. J. R. Astron. Soc.* **68**, 241 (1982).
23. P. J. Gierasch *et al*., *Nature* **403**, 628 (2000).
24. A. Seiff, *Nature* **403**, 603 (2000).

25. Supported by a Particle Physics and Astronomy Research Council and National Science Foundation of China grant (K.Z.) and by the NASA Planetary Atmospheres Program (G.S.).

25 August 2000; accepted 30 October 2000

Rapid Changes in the Hydrologic Cycle of the Tropical Atlantic During the Last Glacial

Larry C. Peterson,[1]* Gerald H. Haug,[2] Konrad A. Hughen,[3] Ursula Röhl[4]

Sedimentary time series of color reflectance and major element chemistry from the anoxic Cariaco Basin off the coast of northern Venezuela record large and abrupt shifts in the hydrologic cycle of the tropical Atlantic during the past 90,000 years. Marine productivity maxima and increased precipitation and riverine discharge from northern South America are closely linked to interstadial (warm) climate events of marine isotope stage 3, as recorded in Greenland ice cores. Increased precipitation at this latitude during interstadials suggests the potential for greater moisture export from the Atlantic to Pacific, which could have affected the salinity balance of the Atlantic and increased thermohaline heat transport to high northern latitudes. This supports the notion that tropical feedbacks played an important role in modulating global climate during the last glacial period.

Large millennial-scale air temperature oscillations first observed in the oxygen isotopic composition ($\delta^{18}O$) of Greenland ice reflect massive reorganizations of the atmosphere-ocean system during the last glacial period (*1*). A growing number of records show that their importance was global in scope (*2*). In the search for mechanisms, attention has increasingly focused on the tropics because of their potential to alter the oceanic balance of heat and fresh water, in addition to their role as a source of water vapor to the atmosphere (*3*). Although precise documentation of changing tropical hydrologies is critical to furthering our understanding of rapid climate variations, only a few locations around the world provide appropriate recorders. Here, we present a multiproxy sediment record of subcentennial resolution that is interpreted to reflect variations in ocean productivity and precipitation patterns over northern South America during the past 90,000 years (90 ky).

The Cariaco Basin is located in a region that is highly sensitive to climate change. Today, upwelling of cold nutrient-rich waters occurs along the northern Venezuelan coast in response to trade wind changes that accompany the seasonal migration of the Intertropical Convergence Zone (ITCZ). The movement of the ITCZ also imposes a wet and dry season on the region, with rainfall variations affecting rivers that deliver terrigenous sediment and nutrients to the western North Atlantic and southern Caribbean. Cariaco Basin sediments record a history of this upwelling and riverine runoff (*4–6*) and offer the opportunity to reconstruct past changes in the tropical ocean and atmosphere and in the hydrologic balance over northern South America.

We report results from Ocean Drilling Program (ODP) Site 1002 (10°42.73′N, 65°10.18′W), drilled at a water depth of 893 m in the basin. The 170-m sediment sequence is continuous and spans the time interval from 0 to ~580,000 years ago (580 ka) (*7*); only data from the uppermost 36 m of Hole 1002C, spanning the period from 0 to 90 ka, are presented here. Terrigenous components compose a large fraction of the sediments (35 to 90 weight %) (*7*) because of the proximity to the South American margin, with variable contributions from nannofossils, foraminifers, diatoms, and pteropods. High sedimentation rates (averaging 40 cm/ky) result in an important tropical counterpart to high-latitude ice cores for the study of rapid climate change.

[1]Rosenstiel School of Marine and Atmospheric Science, University of Miami, Miami, FL 33149, USA. [2]Department of Earth Sciences, Swiss Federal Institute of Technology (ETH), CH-8092 Zürich, Switzerland. [3]Woods Hole Oceanographic Institution, Woods Hole, MA 02543, USA. [4]Fachbereich Geowissenschaften, Universität Bremen, D-28334 Bremen, Germany.

*To whom correspondence should be addressed. E-mail: lpeterson@rsmas.miami.edu

Much of Site 1002 is visibly laminated and devoid of benthic microfauna, indicating deposition under anoxic conditions. However, subsurface intervals showing evidence of bioturbation and containing benthic foraminifers testify to past oscillations between oxic and anoxic conditions in the deep basin (*7*). These oscillations are reflected in sediment color, with laminated intervals appearing as dark green and bioturbated intervals appearing as a light green or yellowish brown.

Measurements of reflectance (*8*) in the "green" wavelength (550 nm) provide a more quantitative view of sediment color (Fig. 1) and reveal a striking resemblance to air temperature variations over Greenland as inferred by $\delta^{18}O$ in the Greenland Ice Sheet Project (GISP) II ice core (*9*). At Site 1002, we used marine isotope stages (MISs) identified from foraminiferal $\delta^{18}O$ (*7*), together with 39 accelerator mass spectrometry (AMS) ^{14}C dates of the foraminifer *Globigerina bulloides* (*10, 11*) to construct a calendar age model that allowed initial correlation of common events in the two records. We then fine-tuned the Cariaco chronology to GISP II $\delta^{18}O$ by visually matching common inflection points and interpolating in between. Over the range of radiocarbon control, the age differences between the ^{14}C-based age model and the tuned age model are within the range of the combined uncertainties of the separate GISP II and calibrated ^{14}C age estimates. Because of this observation and the uncertainties in radiocarbon calibrations before 15 ka, we opted to use the GISP II–based model in this work. Confidence in this approach also comes from earlier work that has demonstrated that gray-scale variations during the last deglaciation in Cariaco cores can be confidently matched to, and are synchronous with, ice core $\delta^{18}O$ changes at the subdecadal level (*5*).

Although the sharp color change accompanying the redox transition at 14.5 ka (12.6 ka in radiocarbon years) and variations within MIS 1 have been previously described (*4, 5*), the long Site 1002 record shows that deposition of dark laminated sediment during the glacial period was apparently coeval with the interstadial warmings recorded at the GISP II site (Fig. 1). In contrast, cold periods in Greenland were marked by the accumulation of light-colored bioturbated sediments in the Cariaco Basin. This record of variation in color and laminae distribution (and the implied linkage to high-latitude North Atlantic climate) is essentially identical to that observed in the Santa Barbara Basin and along the California margin (*12*) and, more recently, off Pakistan (*13*). However, unlike these locations where oxygen minimum zone (OMZ) fluctuations have been invoked to explain the presence or absence of laminations, the shallow sill depth (146 m at present) of the Cariaco Basin effectively precludes similar OMZ scenarios. This is especially true for glacials when lowered sea levels would have led to yet shallower sill depths of ~25 to 70 m, limiting the source of water to the basin to the well-mixed and oxygenated waters of the near-surface region.

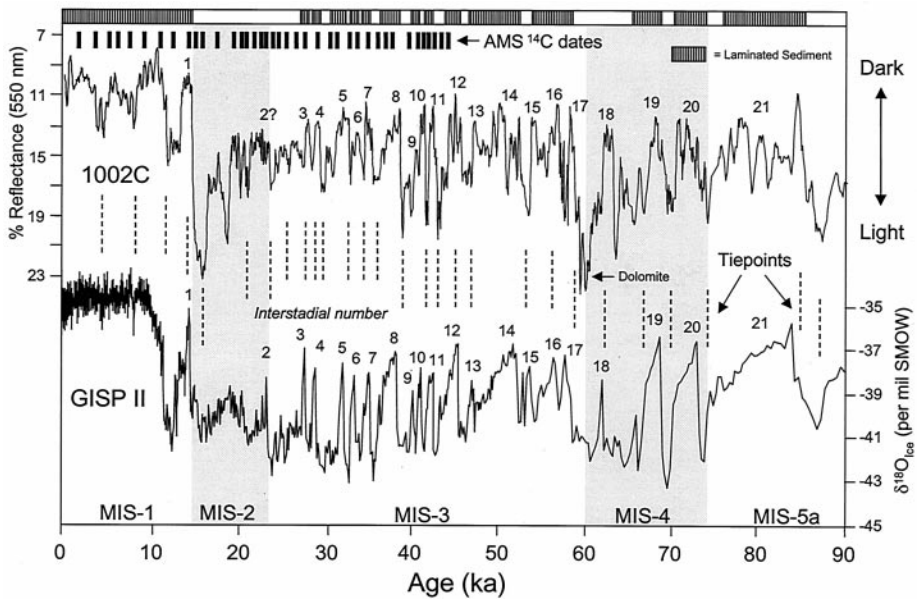

Fig. 1. Comparison of measured color reflectance (550 nm) (five-point moving average) of Cariaco Basin sediments from ODP Hole 1002C to $\delta^{18}O$ from the GISP II ice core (*9*). MIS boundaries in Hole 1002C are from (*7*), and detailed age control over the upper 22 m is based on AMS ^{14}C dating of the planktic foraminifer *G. bulloides* (*10*). Additional visual tie points between the color reflectance and GISP $\delta^{18}O$ records are shown. The distribution of laminated intervals is indicated across the top. The presence of a semi-indurated dolomite layer in Hole 1002C at 28.3 m below the sea floor resulted in minor core disturbance at this level. Deposition of dark, generally laminated sediments preferentially occurs during warm interglacial or interstadial times (numbered events), whereas deposition of light-colored bioturbated sediments was restricted to colder stadial intervals of the last glacial. Sediment color variations in the Cariaco Basin are driven by changing surface productivity, with increased organic rain leading to darker sediments and, through remineralization reactions, periods of anoxic or near-anoxic conditions in the deep basin. SMOW, standard mean ocean water.

Color and laminae distribution are but two of a number of Cariaco properties that show linkage to the ice core record. Within MIS 3, variations in the bulk Fe, Ti, and Ca content of Site 1002 sediments also show a strong relation to events recorded in the Greenland ice. High-resolution elemental measurements in this interval were obtained with a profiling x-ray fluorescence (XRF) scanner (*14, 15*). High Fe and Ti intensities are closely associated with the dark laminated sediments deposited during interstadial times (Figs. 2 and 3), whereas Ca values show the opposite pattern (Fig. 3). Although the Fe behavior alone might be attributed to the parallel redox changes in the sediment, Ti behavior, which is redox-insensitive (*16*), shows an identical downcore pattern. Hence, Fe and Ti variations in the Cariaco Basin are not diagenetically controlled and are interpreted to reflect changes in input of fine terrigenous (siliciclastic) components. High Ca intensities, on the other hand, reflect the $CaCO_3$ content of the sediments, which is mostly derived from coccoliths and planktic foraminifers.

Color variations at Site 1002 are dominantly controlled by total organic carbon (TOC), with high TOC values associated with darker, less reflective sediment (*7*). On glacial-interglacial time scales, TOC fluctuations at Site 1002 (0.1 to 5%) have been previously interpreted to reflect the first-order history of export productivity in the Cariaco Basin (*17*), with sea level playing an important role in modulating that production. During glacials, lowered sea levels would have increasingly isolated the Cariaco Basin and restricted input of nutrient-rich subsurface waters, thus limiting production and reducing O_2 consumption from the remineralization of sinking organic detritus (*6, 17*). In contrast, high interglacial sea levels increase the supply of nutrients from the open Caribbean, stimulating productivity and contributing to the anoxic depositional conditions that prevailed at these times (*7*).

Are the millennial-scale variations in sediment color and lamination occurrence reported here for the glacial interval (Fig. 1) also a reflection of changing surface productivity? At first glance, the low Ca contents of the dark laminated sediments deposited during interstadials (Fig. 3) might seem to indicate low productivity of calcareous plankton. However, preliminary foraminiferal data in

fact suggest the opposite, with high abundances of the productivity indicator *G. bulloides* found in the laminated intervals (*18*). Increased carbonate dissolution, another possibility for explaining low interstadial Ca values, is ruled out by the fact that aragonitic pteropods are common throughout the sequence and foraminiferal preservation is excellent. The striking inverse relation between Ca and Fe in these sediments instead suggests that dilution plays the major role in their respective downcore distributions. In order to test this and to avoid the closed-sum problems inherent in the raw data, we calculated Fe and $CaCO_3$ accumulation rates (g/cm^2 per ky) for the well-constrained interval encompassing interstadials 3 through 7 (Fig. 3) (*19*). In contrast to the intensity data, these calculations suggest that the accumulation of both $CaCO_3$ and detrital Fe largely increased and decreased in concert during this portion of MIS 3. We interpret these results to indicate both higher biological productivity and increased terrigenous input to the Cariaco Basin during interstadial times.

Millennial-scale variability in surface production presumably requires a mechanism related to circulation and/or nutrient supply, rather than being driven by sea level. Although a number of studies have focused on the history of trade wind–induced upwelling over the Cariaco Basin within MIS 1 (*4–6, 20*), we consider it unlikely that upwelling is responsible for the abrupt productivity changes observed during the last glacial along the Venezuelan coast. Today, coastal upwelling over the Cariaco Basin is strongest during Northern Hemisphere winters when North Atlantic sea surface temperatures (SSTs) are cool in relation to those in the South Atlantic. Cooler North Atlantic SSTs result in increased surface pressure over the North Atlantic and a southward shift of the ITCZ (*21*), with intensified northeasterly trade winds driving stronger upwelling over the basin. Studies of the Younger Dryas (*5*), as well as studies of recent decadal-scale changes calibrated to instrumental data (*20*), indicate intensification of upwelling over the Cariaco Basin at times of cooler North Atlantic SSTs, suggesting a coherent climatological response on longer time scales that is simply an enhancement of the annual cycle. During the last glacial, evidence for stronger northeasterly trade winds and southward displacement of the ITCZ comes from both data and modeling studies (*22, 23*). Although one might predict more intense upwelling over the Cariaco Basin as a result, nutrient limitations imposed by lower sea level and shallower sills appear to have kept glacial productivity levels generally below those of the Holocene and earlier interglacials (*4, 7*). Superimposed on this background of low glacial productivity are the millennial-scale productivity peaks implied by the Site 1002 reflectance data (Fig. 1). If these were driven solely by trade wind–induced upwelling, one might expect a relation between productivity maxima and the cold stadial intervals of the North Atlantic. In fact, the opposite is observed.

We hypothesize that the millennial-scale productivity pulses recorded in the Cariaco Basin during the last glacial are not the result of upwelling, but rather of an increased supply of river-borne nutrients to the coastal waters of northern South America, with the primary evidence for varying riverine influence coming from the bulk Fe and Ti signals in Site 1002. High Fe and Ti abundances during periods of warm interstadial climate indicate increased terrigenous input to the Cariaco Basin and imply higher rainfall and increased runoff from the watersheds of rivers that affect the basin.

A number of small rivers drain the coast bordering the Cariaco Basin, but these rivers are located today ~50 km or more from the basin itself and discharge directly onto a broad shallow shelf (<50 m), where their sedimentary contributions are largely trapped (*24*). The eastern Caribbean and Cariaco Basin at present also receive an input of fine-grained siliciclastics from the Orinoco-Amazon plume (*25*). During glacial lowstands of sea level, the shelf around the Cariaco Basin was reduced to a few kilometers in width, and direct input of sediment from local rivers was volumetrically more substantial in relation to Orinoco-Amazon sources (*16, 25*). We suggest that the combination of greatly reduced shelf width and area during lowstands resulted in glacial-age sediments of the Cariaco Basin being more sensitive to fluctuations in terrigenous input driven by rainfall-related changes in riverine discharge. In addition, the shifting of river mouths to near the edge of the basin may have led to locally amplified effects on surface productivity from river-sourced nutrients.

Pollen records from both marine and terrestrial sequences in northern South America suggest arid conditions and extensive savanna vegetation in the northern coastal region toward the end of the last glacial (*26*). For the period before ~15 ka, little direct terrestrial information is available on climatic conditions along the northern coast, although at least one modeling study predicts increased precipitation during interstadials when warmer North Atlantic SSTs are prescribed (*27*). Together, data presented here and data from a lower resolution sediment record off northeastern Brazil (*28*) indicate a broad regional signal of millennial-scale changes in the water balance over tropical South America not previously identified in terrestrial records. These changes are consistent with variations in SST gradients and ITCZ behavior that might be expected from atmosphere-oceanice interactions originating in the North At-

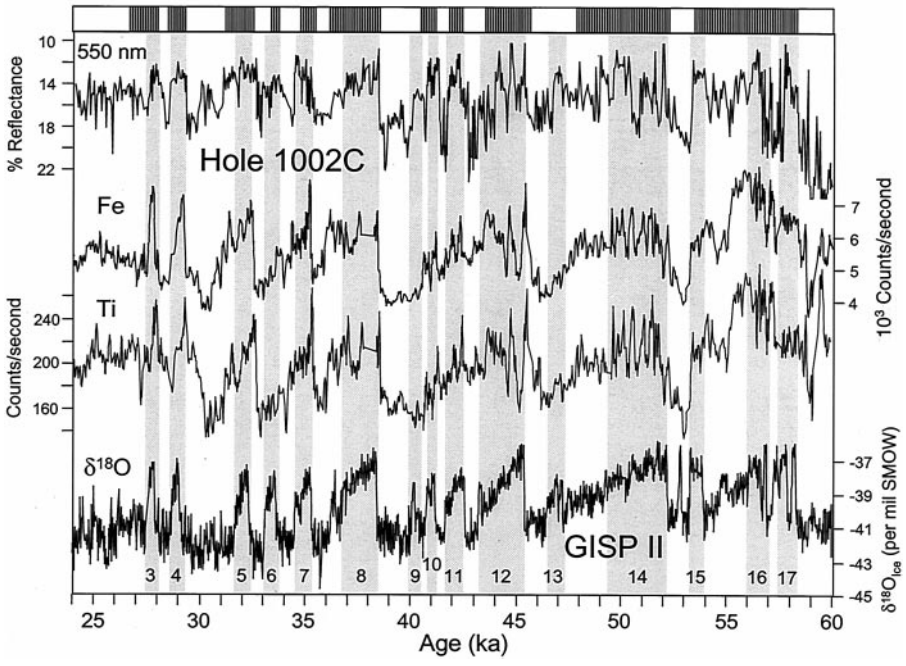

Fig. 2. Detailed comparison of sediment reflectance and Fe and Ti (counts/s) (three-point moving average) from MIS 3 sediments of ODP Hole 1002C with measured $\delta^{18}O$ in the GISP II ice core (*9*). The distribution of laminated sediment intervals in MIS 3 is shown across the top of the figure. Warm interstadials in the GISP II record were marked by the deposition of Fe- and Ti-rich, dark, and generally laminated (anoxic) sediments in the Cariaco Basin. High Fe and Ti values indicate periods of greater terrigenous input to the basin and reflect increased precipitation and input from rivers draining the northern coast of tropical South America.

lantic. Furthermore, the evidence for higher interstadial precipitation over at least this one region highlights the potential importance of tropical water vapor, a key greenhouse gas, in helping to globally amplify abrupt climate changes.

In addition to providing direct evidence for rapid hydrologic changes during the last glacial, data from the Cariaco Basin also point to a potential role of the tropics as a source of millennial-scale climatic variability. Although the Site 1002 data reflect change in only one small part of the world, they capture variability in a region where changing water balances may play a pivotal role in generating extratropical feedbacks. A number of modeling studies have noted the sensitivity of thermohaline circulation to changes in atmospheric moisture transport from the Atlantic to Pacific Ocean (*29, 30*). In general, a net export of moisture makes the Atlantic saltier and favors deepwater formation in the North Atlantic. In the tropical Atlantic, the narrow and relatively low Isthmus of Panama is the prime pathway for atmospheric moisture loss to the Pacific (*31*). During warm interstadials, increased precipitation affected river discharge into the Cariaco Basin, which lies at approximately the latitude of the low-lying Panamanian land bridge. We speculate that higher interstadial rainfall along the northern coastline of South America may have led to a higher net export of moisture to the Pacific, thus enhancing the Atlantic-Pacific salinity contrast and increasing thermohaline heat transport to the high northern latitudes. During colder stadials, drier conditions over northern South America might be explained by a modest southward shift of the ITCZ and its belt of convective rainfall away from the low-lying Isthmus of Panama and into mountainous Andean terrain. This could have led to orographic rainfall and moisture "blocking" by the Andes and an overall drop in freshwater export to the Pacific, leading to reduced thermohaline overturning and decreased northward heat transport. Alternatively, changes in the inferred location of tropical convection might be a response to forcing outside the Atlantic. During warm El Niño events, for example, the SST structure of the tropical Pacific becomes more symmetric around the equator, and the mean ITCZ position in that basin shifts to the south (*32*). This has global effects on temperature and precipitation patterns in the tropics and extratropics (*33*). Whether the tropical Pacific plays a role in generating millennial-scale hydrologic changes over northern South America remains to be seen. Either scenario suggests the potential for strong tropical feedbacks in the generation of abrupt climate changes; such mechanisms need to be tested by further data collection and climate modeling.

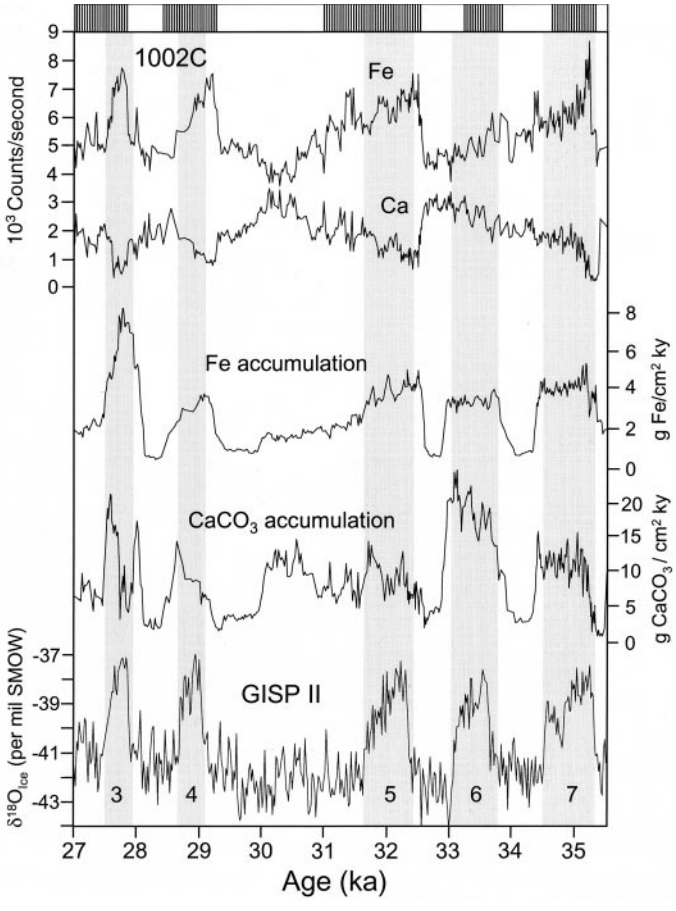

Fig. 3. Variations in XRF intensities (counts/s) (top) for Fe and Ca (*14*) over the time interval from ODP Hole 1002C encompassing interstadials 3 through 7 in the GISP II record (bottom). The distribution of laminated sediment intervals is shown across the top of the figure. Measured Fe intensities reflect the relative abundance of terrigenous components in the sediment, whereas Ca values are highly correlated to biogenic carbonate contents. Measured intensity values were combined with sedimentation rate information from the age model and DBD data to calculate Fe and equivalent $CaCO_3$ accumulation rates (middle) for this interval (*19*). These calculations indicate that the accumulation of both Fe and $CaCO_3$ increased in the Cariaco Basin during warm interstadial periods. The peaks in terrigenous input are interpreted to reflect intervals of increased regional precipitation and riverine discharge, with higher (carbonate) productivity likely driven by the introduction of new river-sourced nutrients directly into the basin.

References and Notes

1. G. Bond *et al.*, *Nature* **365**, 143 (1993).
2. P. U. Clark, R. S. Webb, L. D. Keigwin, Eds., *Mechanisms of Global Climate Change at Millennial Time Scales*, vol. 112 of *Geophysical Monograph Series* (American Geophysical Union, Washington, DC, 1999).
3. W. S. Broecker, *Global Biogeochem. Cycles* **11**, 589 (1997).
4. L. C. Peterson, J. T. Overpeck, N. G. Kipp, J. Imbrie, *Paleoceanography* **6**, 99 (1991).
5. K. A. Hughen, J. T. Overpeck, L. C. Peterson, S. E. Trumbore, *Nature* **380**, 51 (1996).
6. H.-L. Lin, L. C. Peterson, J. T. Overpeck, S. E. Trumbore, D. W. Murray, *Paleoceanography* **12**, 415 (1997).
7. L. C. Peterson *et al.*, *Proc. Ocean Drill. Program Sci. Results* **165**, 85 (2000).
8. Color measurements were made at 2-cm intervals on fresh, cleaned core surfaces using a handheld Minolta CM-2002 spectrophotometer. The Minolta CM-2002 measures reflected visible light in 31 10-nm-wide spectral bands ranging from 400 to 700 nm.
9. M. Stuiver, P. M. Grootes, *Quat. Res.* **53**, 277 (2000).
10. AMS ^{14}C dates were generated on monospecific samples of *G. bulloides* at ~0.5-m intervals from the upper 22 m of ODP Hole 1002D. AMS dates were then transferred to Hole 1002C through detailed color and physical property correlations. All measurements were done at the Center for AMS (Lawrence Livermore National Laboratory, Livermore, CA). AMS ^{14}C dates were corrected by a known reservoir age of 420 years (*5*) and converted to calendar ages by using the calibration of (*11*).
11. E. Bard, M. Arnold, R. G. Fairbanks, B. Hamelin, *Radiocarbon* **35**, 191 (1993).
12. R. J. Behl, J. P. Kennett, *Nature* **379**, 243 (1996).
13. H. Schulz, U. von Rad, H. Erlenkeuser, *Nature* **393**, 54, (1998).
14. The chemical elemental composition of MIS 3 sediments was analyzed at a 1-cm resolution using an XRF core scanner at the University of Bremen. The XRF profiling scanner was developed and built at the Netherlands Institute for Sea Research (Texel, Netherlands) and is a nondestructive analysis system for scanning the archive half of split sediment cores. Details on the general method and calibration procedures can be found in (*15*).
15. J. H. F. Jansen, S. J. van Der Gaast, B. Koster, A. J. Vaars, *Mar. Geol.* **151**, 143 (1998).
16. K. M. Yarincik, R. W. Murray, L. C. Peterson, *Paleoceanography* **15**, 210 (2000).
17. G. H. Haug *et al.*, *Paleoceanography* **13**, 427 (1998).
18. C. O'Hara, L. C. Peterson, unpublished data.
19. Mass accumulation rates for Fe and $CaCO_3$ in the interval encompassing interstadials 3 through 7 in Hole 1002C were calculated by taking the product of the elemental abundances for Fe and Ca at each measurement depth, the dry bulk density (DBD) of the sediment, and the sedimentation rate. Sedimentation rate estimates (in cm/ky) were derived from the GISP II–tuned age model. Measured XRF intensity values were converted to elemental abundance values by using the following formulas based on calibration of both standards and replicate sediment analyses: parts per million Fe = Fe counts/s × 7.11; % $CaCO_3$ = (Ca counts/s × 0.0053) + 5.0. DBD values (in g/cm^3) for each sample depth were estimated from shipboard GRAPE (gamma-ray attenuation porosity evaluation) density measurements by the formula DBD = (GRAPE density − 1.0532)/0.4932.
20. D. E. Black *et al.*, *Science* **286**, 1709 (1999).
21. S. Hastenrath, L. Greischar, *J. Geophys. Res.* **98**, 5093 (1993).
22. S. E. Harris, A. C. Mix, *Quat. Res.* **51**, 14 (1999).
23. A. J. Broccoli, *J. Clim.* **13**, 951 (2000).

24. N. J. Maloney, *Bol. Inst. Oceanogr. Univ. Oriente* **4**, 246 (1965).
25. T. Clayton, R. B. Pearce, L. C. Peterson, *Mar. Geol.* **161**, 191 (1999).
26. C. Schubert, *Interciencia* **13**, 128 (1988).
27. S. W. Hostetler, P. U. Clark, P. J. Bartlein, A. C. Mix, N. J. Pisias, *J. Geophys. Res.* **104**, 3947 (1999).
28. H. W. Arz, J. Pätzold, G. Wefer, *Quat. Res.* **50**, 157 (1998).
29. T. F. Stocker, D. G. Wright, *Nature* **351**, 729 (1991).
30. F. Zaucker, T. F. Stocker, W. S. Broecker, *J. Geophys. Res.* **99**, 12443 (1994).
31. P. K. Weyl, *Meteorol. Monogr.* **8**, 37 (1968).
32. A. V. Fedorov, S. G. Philander, *Science* **288**, 1997 (2000).
33. M. Cane , A. C. Clement, in (*2*), pp. 373–383.
34. This research was supported by the U.S. NSF (Division of Ocean Sciences) and the Deutsche Forschungsgemeinschaft. We thank A. Clement and C. Rooth for valuable discussion and J. Kennett and two anonymous referees for their thorough reviews. This work was made possible by the ODP and the efforts of the scientific party and crew of ODP Leg 165. This is a contribution from the Rosenstiel School of Marine and Atmospheric Science, University of Miami.

14 August 2000; accepted 9 November 2000

Synchronous Radiocarbon and Climate Shifts During the Last Deglaciation

Konrad A. Hughen,[1]* John R. Southon,[2] Scott J. Lehman,[3] Jonathan T. Overpeck[4]

Radiocarbon data from the Cariaco Basin provide calibration of the carbon-14 time scale across the period of deglaciation (15,000 to 10,000 years ago) with resolution available previously only from Holocene tree rings. Reconstructed changes in atmospheric carbon-14 are larger than previously thought, with the largest change occurring simultaneously with the sudden climatic cooling of the Younger Dryas event. Carbon-14 and published beryllium-10 data together suggest that concurrent climate and carbon-14 changes were predominantly the result of abrupt shifts in deep ocean ventilation.

Efforts to calibrate the radiocarbon time scale and to quantify the record of changes in past atmospheric ^{14}C concentration [$\Delta^{14}C$, reported as per mil (‰) deviations from the preindustrial value] rely primarily on ^{14}C measurements on tree-ring dated wood (*1*, *2*). However, these dendrochronological records extend back only to ~11,900 calendar years before present (11.9 cal kyr B.P.) and do not provide calibration during most of the large, abrupt climate changes of the last deglaciation, including the Younger Dryas cold reversal. Paired U/Th-^{14}C dates from corals have been used to extend ^{14}C calibration back in time beyond that determinable by tree rings (*3*–*6*), revealing elevated $\Delta^{14}C$ during the Younger Dryas period. However, available ^{14}C calibration data from corals provide limited temporal resolution and do not constrain the decade-century scale details of past ^{14}C variation. Recently reported results (*7*) documenting abrupt changes in $\Delta^{14}C$ and climate during the onset of the Younger Dryas are consistent with the hypothesis that a shutdown of deep ocean ventilation caused shifts in both ^{14}C and climate (*7*–*11*). However, those data are not of high enough resolution to conclusively determine the timing of the $\Delta^{14}C$ shift relative to the Younger Dryas onset, leading to speculation that the $\Delta^{14}C$ changes were caused by another mechanism (e.g., solar variability) (*12*). Here we present ^{14}C data from Cariaco Basin core PL07-58PC (hereafter 58PC), providing 10- to 15-year resolution through most of deglaciation. The new calibration data demonstrate conclusively that $\Delta^{14}C$ changes were synchronous with climate shifts during the Younger Dryas. Calculated $\Delta^{14}C$ is strongly correlated to climate proxy data throughout early deglaciation ($r = 0.81$). Comparing $\Delta^{14}C$ and ^{10}Be records leads us to conclude that ocean circulation changes, not solar variability, must be the primary mechanism for both ^{14}C and climate changes during the Younger Dryas.

Cariaco Basin core 58PC (10°40.60′N, 64°57.70′W; 820 m depth) has an average sedimentation rate (70 cm/kyr) more than 25% higher than core 56PC (10°41.22′N, 64°58.07′W; 810 m depth) (*13, 14*), and shares similar hydrographic conditions. Restricted deep circulation and high surface productivity in the Cariaco Basin off the coast of Venezuela create an anoxic water column below 300 m. The climatic cycle of a dry, windy season with coastal upwelling, followed by a nonwindy, rainy season, results in distinctly laminated sediment couplets of light-colored, organic-rich plankton tests and dark-colored mineral grains from local river runoff (*13*). It has been demonstrated previously that the laminae couplets are annually deposited varves and that light laminae thickness, sediment reflectance (gray scale), and abundance of the foraminifer *Globigerina bulloides* are all sensitive proxies for surface productivity, upwelling, and trade wind strength (*14*, *15*). Nearly identical patterns, timing, and duration of abrupt changes in Cariaco Basin upwelling compared with surface temperatures in the high-latitude North Atlantic region at 1- to 10-year resolution during the past 110 years and the last deglaciation (*7*, *14*, *15*) provide evidence that rapid climate shifts in the two regions were synchronous. A likely mechanism for this linkage is the response of North Atlantic trade winds to the equator-pole temperature gradient forced by changes in high-latitude North Atlantic temperature (*16*).

The hydrography of the Cariaco Basin provides excellent conditions for ^{14}C dating (*17*). The shallow sills (146 m depth) constrain water entering the basin to the surface layer, well equilibrated with atmospheric CO_2. Despite anoxic conditions, the deep waters of the Cariaco Basin have a brief residence time, as little as 100 years (*17*). Two radiocarbon dates on *G. bulloides* of known recent calendar age gave the same surface water-atmospheric ^{14}C difference (reservoir age) as the open Atlantic Ocean (*7*). Good agreement during the early Holocene and Younger Dryas between Cariaco Basin and terrestrial ^{14}C dates, including German pines and plant macrofossils from lake sediments (*1*, *9*, *11*, *18*) (Fig. 1), suggests that Cariaco Basin reservoir age does not change measurably as a response to increased local upwelling (i.e., during the Younger Dryas) (*19*). Planktonic foraminiferal abundance permits continuous sampling at 1.5-cm increments, providing 10- to 15-calendar-year resolution throughout most of deglaciation.

For this work, the varve chronology is largely the same as that used for core 56PC (*7*). Varves have been re-counted during periods of particular importance, such as the overlap with tree rings and the onset of the Younger Dryas, as well as the deepest, oldest laminations that are less distinct. The floating Cariaco Basin varve chronology was anchored to the German pine dendrochronology by wiggle-matching ^{14}C variations in both curves (Fig. 1). The correla-

[1]Department of Marine Chemistry and Geochemistry, Woods Hole Oceanographic Institution, Woods Hole, MA 02543, USA. [2]Center for Accelerator Mass Spectrometry, Lawrence Livermore National Laboratory, Livermore, CA 94551, USA. [3]Institute of Arctic and Alpine Research and Department of Geological Sciences, University of Colorado, Boulder, CO 80309, USA. [4]Institute for the Study of Planet Earth and Department of Geosciences, University of Arizona, Tucson, AZ 85721, USA.

*To whom correspondence should be addressed. E-mail: khughen@whoi.edu

Rapid Changes in the Hydrologic Cycle of the Tropical Atlantic During the Last Glacial

Larry C. Peterson *et al.*

Science **290**, 1947 (2000);
DOI: 10.1126/science.290.5498.1947